A Hybrid Control Strategy for CLLLC Resonant Converter Based on PS-PFM under Wide Input Voltage

Minghai Xie
Department of Electrical Engineering
(*Jiangnan University*)
Wuxi, China
xieminghai1999@163.com

Kaitao Bi
Department of Electrical Engineering
(*Jiangnan University*)
Wuxi, China
bkt1989@163.com

Jian Ai
Department of Electrical Engineering
(*Jiangnan University*)
Wuxi, China
jianai0204@126.com

Qigao Fan
Department of Electrical Engineering
(*Jiangnan University*)
Wuxi, China
qgfan@jiangnan.edu.cn

2023 26th International Conference on Electrical Machines and Systems (ICEMS) | 979-8-3503-1758-9/23/$31.00 ©2023 IEEE | DOI: 10.1109/ICEMS59686.2023.10344382

***Abstract*- This paper focuses on the CLLLC resonant converter as the research object which faces challenges such as narrow input voltage range, wide range of switching frequency variation, and difficulty in achieving soft switching. To address these issues, a hybrid modulation method based on PS-PFM is proposed in this paper, which jointly controls the switching frequency and phase-shift angle. By analyzing the necessary condition of CLLLC resonant converter for achieving zero voltage switching (ZVS), the expression for the relationship between the switching frequency and the phase shift angle is derived. Compared to traditional pulse frequency modulation (PFM) and phase-shift modulation (PSM), this method can significantly expand the input voltage range while ensuring ZVS of the switches and a narrow range of switching frequency variation. The effectiveness of the proposed control method was validated through an 800W prototype.**

Keywords—CLLLC Resonant Converter, ZVS, PS-PFM, Hybrid Control.

I. INTRODUCTION

In recent years, bidirectional DC-DC converters have been widely used in new energy equipment such as energy storage systems and on-board chargers due to their ability to enable bidirectional energy flow. Bidirectional DC-DC converters can be classified into isolated and non-isolated types based on the presence of a high-frequency transformer. The following are common types of isolated DC-DC converters: dual active bridge (DAB) converter, bidirectional LLC resonant converter, and CLLLC resonant converter. The topology and control method of DAB converter are simple, as it only changes the phase shift angle between the primary side and secondary side to control the voltage gain and energy flow. However, DAB has large turn-off loss and it is difficult to achieve ZVS, resulting in low efficiency. The bidirectional LLC resonant converter adds resonant inductor and resonant capacitor to the DAB structure, which allows for zero voltage switching (ZVS) of the primary side switches and zero current switching (ZCS) of the secondary side body diodes. As a result, the efficiency of converter is improved. However, the bidirectional LLC resonant converter can only achieve buck mode when energy is transferred in reverse, limiting its application scenarios. [1] proposed a bidirectional three-level LLC resonant converter, however, the excessive number of switches and flying capacitors limits its power density. Compared to the previous topologies, the CLLLC resonant converter has the advantages of bidirectional buck/ boost due to its symmetrical resonant tank.

At present, many modulation methods have been adopted in resonant converter, such as pulse frequency modulation (PFM), symmetrical pulse width modulation (SPWM), asymmetrical pulse width modulation (ASPWM) and phase-shift modulation (PSM). PFM is the conventional modulation method, which adjusts the voltage gain of the converter by varying the switching frequency of the switching transistor. However, when the converter has large input voltage range or under light load, only switching frequency can be controlled to maintain the output voltage, which will increase power loss. APWM, SPWM, and PSM respectively regulate the voltage gain by adjusting the duty cycle of driving signal or the phase shift angle between switching bridge arms of the primary side. However, they can only achieve boost or buck regulation. [2] proposed a segmentation control method combining PFM and PSM, where PFM is responsible for boost regulation, and PSM is responsible for buck regulation. However, it is difficult to determine the switching point between PFM and PSM. On the other hand, the converter loses ZVS characteristic under large phase shift angle. To further increase the input voltage range and reduce the range of switching frequency variation, [3] proposed a variable-mode control method based on APWM, PFM, and SPWM. APWM, PFM, and SPWM is assigned to the high-gain, mid-gain, and low-gain region , respectively. However, hysteresis switching needs to be implemented between different modulation methods, which increases the complexity of control. [4] and [5] proposed a smooth and flexible variable modal control strategy based on PFM, phase-shift asymmetry control (PSAS) and doubled PWM (DPWM). By adding the PSAS mode between PFM and DPWM, flexible and smooth transitions between the three modes are achieved. The control method proposed in [6] and [7] integrates PFM and PSM to regulate output voltage and ensure ZVS operation. PFM is responsible for achieving ZVS operation of the switching transistors within the full load range while PSM is responsible for regulating voltage gain. To solve the problem of limited frequency resolution of DSP, a control method combining PWM and PFM was proposed in [8], which significantly reduces the steady-state error of voltage and current spikes, thus improving the steady-state performance of the converter. The control methods proposed in [6], [7] and [8] are frequency and duty cycle or frequency and phase-shift angle hybrid control. Although they achieve soft switching under wide voltage gain, the complexity of the control strategy limits their applications in engineering.

To balance the effectiveness and simplicity of control method, this paper proposes a hybrid control strategy based on PS-PFM, which extends the voltage gain range within a narrow switching frequency range and achieves ZVS for the primary-side switches and ZCS for the secondary-side switches, thereby improving the efficiency of the converter.

II. Operational Principle

A. topology of CLLLC resonant converter

Fig.1 is the topology of the CLLLC resonant converter, which consists of primary-side full bridge, resonant tank and secondary-side full bridge. The primary-side full bridge and secondary-side full bridge is composed of MOSFET Q_1-Q_4, and Q_5-Q_8, respectively. D_1-D_8 and C_{s1}-C_{s8} represent the body diodes and parasitic capacitors of the MOSFETs, which provide conditions for achieving ZVS. The resonant tank consists of the primary and secondary resonant inductors (L_1, L_2), resonant capacitors (C_1, C_2), magnetic inductance L_m. The turns ratio high-frequency transformer T_r is n:1.

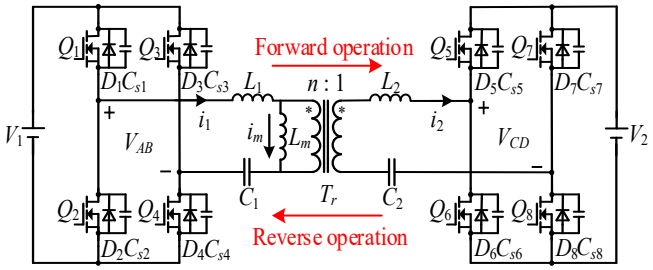

Fig.1. Topology of the CLLLC resonant converter.

When the converter is in forward operation, the primary-side switches are driven as an inverter and the secondary-side full bridge rectification is implemented by body diodes, and vice versa. The primary and secondary side resonant components are designed with symmetric parameters to facilitate parameter design and ensure consistency in forward and reverse operation, which means $L_1=n^2L_2$, $C_1=C_2/n^2$.

B. Operational modes

The CLLLC resonant converter has two resonant frequencies, namely series resonant frequency f_r and series-parallel resonant frequency f_m, as shown in equation (1) and (2). When the switching frequency f_s is greater than f_m and less than f_r, the converter operates in under-resonant state. When f_s is equal to f_r, the converter operates in quasi-resonant state. When f_s is greater than f_r, the converter operates in over-resonant state. The PS-PFM modulation method proposed in this paper adjusts the voltage gain by simultaneously changing f_s of the primary side switches and the phase-shift angle φ between the arms of the primary side bridge. Fig.2 is the working waveform under PS-PFM control. Due to the symmetry of the waveforms in the first and second half cycles, we only analyze the working mode of the first half cycle in under-resonant state.

$$f_r = \frac{1}{2\pi\sqrt{L_1C_1}} \tag{1}$$

$$f_m = \frac{1}{2\pi\sqrt{(L_1+L_m)C_1}} \tag{2}$$

Mode 1 (t_1-t_2): Before t_1, the switch Q_3 is turned on. At t_1, Q_3 is turned off. At this moment, the resonant current i_1 start to charge C_{S3} and discharges C_{S4} until t_2.

Mode 2 (t_2-t_4): At t_2, the voltage of C_{S3} rises to V_1 and the voltage of capacitor C_{S4} drops to zero. At this point, the input voltage of the resonant tank V_{AB} is equal to the input voltage V_1. From t_2 to t_4, i_1 is higher than the current of magnetic inductor i_m, indicating energy is transferred from the primary side to the secondary side. During the time period of t_2-t_3, D_4 conducts until V_{G4} transfer to high. As a result, Q_4 achieved ZVS.

Mode 3 (t_4-t_6): At t_4, i_1 is equal to i_m and the primary side stops transferring energy to the secondary side. Therefore, D_5 and D_8 achieve ZCS and L_1, L_m, and C_1 are in series-parallel resonance. At t_5, V_{G1} is low. During t_5-t_6, i_1 charges C_{S1} and discharges C_{S2} until the voltage of C_{S1} reaches V_1 and the voltage of C_{S2} is zero. At this moment, i_1 flows through D_2, causing V_{AB} to drop to zero.

Mode 4 (t_6-t_8): During t_6-t_7, D_2 and Q_4, along with the resonant tank, form a circuit. Due to V_{AB} being zero, the energy in resonant tank is released. As a result, i_1 starts to decrease slowly. At t_7, V_{G2} switches to high level. As a result, Q_2 realize ZVS.

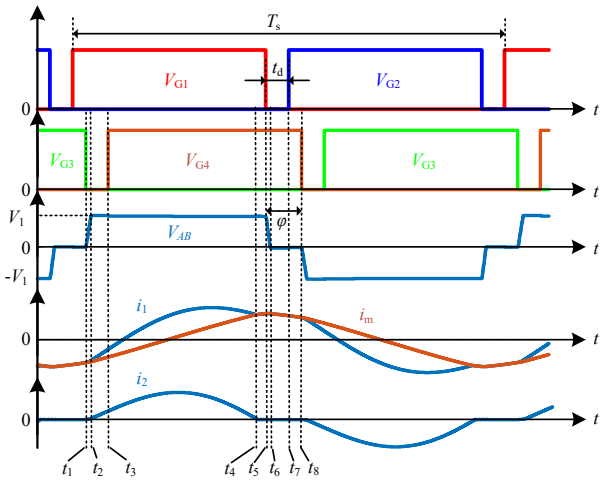

Fig.2. The working waveform under PS-PFM control.

C. Output voltage gain

In order to balance accuracy and convenience in analysis, this paper adopts fundamental harmonic approximation (FHA) method to analyze the CLLLC resonant converter. Fig.3 shows the fundamental harmonic equivalent model of the CLLLC resonant converter during forward operation. In this model, L_2^* and C_2^* respectively represent the equivalent resonant inductor and equivalent resonant capacitor converted to the primary side. Their values satisfy $L_1=L_2^*$, $C_1=C_2^*$. $v_{AB(1)}$ represents the fundamental component of V_{AB}, and R_{eq}^* is the equivalent resistance converted to the primary side. The expressions of them are shown in equation (3) and (4).

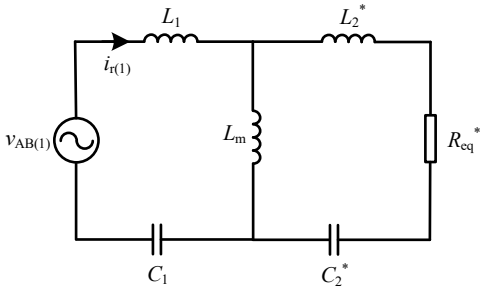

Fig.3. The fundamental harmonic equivalent model of CLLLC resonant converter under forward operation.

$$v_{AB(1)}(t) = \frac{4V_1\cos\frac{\varphi}{2}}{\pi}\sin(\omega_s t - \frac{\varphi}{2}) \tag{3}$$

$$R_{eq}^{*}=\frac{8n^2V_2^2}{\pi^2P_o} \tag{4}$$

According to Fig.3, the voltage gain of the CLLLC resonant converter under forward operation with PS-PFM control can be derived as shown in Equation (5), where the inductance turns ratio is k=L_m/L_1, the normalized switching frequency is f_n=f_s/f_r, and the quality factor $Q=\sqrt{L_1/C_1}\big/R_{eq}^{*}$. Based on (5), the three-dimensional surface plot of the voltage gain M of the CLLLC resonant converter with respect to f_n and φ is shown below. It can be observed that changing f_n individually results in a small range of voltage gain regulation. On the other hand, increasing φ can only achieve buck operation. Therefore, it is necessary to simultaneously change both f_n and φ to achieve a wide voltage gain range.

$$M=\frac{\cos\frac{\varphi}{2}}{\sqrt{(1+\frac{1}{k}-\frac{1}{kf_n^{2}})^2+(\frac{Q}{k})^2[(2k+1)f_n-\frac{2k+2}{f_n}+\frac{1}{f_n^{3}}]^2}} \tag{5}$$

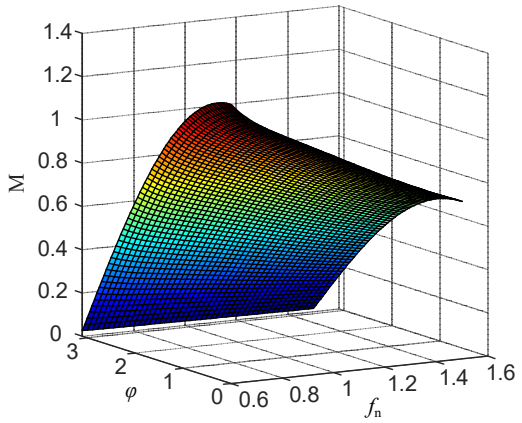

Fig.4. Diagram of voltage gain of CLLLC converter.

III. Hybrid Control Strategy Based on PS-PFM

A. Implementation of PS-PFM

As analyzed in Section II.C, in order to reduce the switching frequency while expanding the range of input voltage variation range, the proposed PS-PFM in this paper enlarges the voltage gain regulation range by simultaneously changing the switching frequency f_s and the phase shift angle φ. This method eliminates the need to switch modulation method based on the magnitude of voltage gain, which is beneficial for stable operation and easy implementation of the converter. Fig.5 shows the closed-loop control block diagram of the PS-PFM. The output of the PI controller determines f_s, and the driving signal for the leading leg is obtained through a voltage-controlled oscillator (VCO). The phase shift φ is obtained through the linear relationship shown in equation (6), and then the driving signal for the lagging bridge arm is obtained through the phase-shifting modulator. The coefficients K and B in equation (6) directly determine whether the switching transistors can achieve ZVS and influence the range of input voltage. In the subsequent sections of this paper, suitable parameter values will be designed based on the ZVS condition.

$$\varphi=Kf_s+B \tag{6}$$

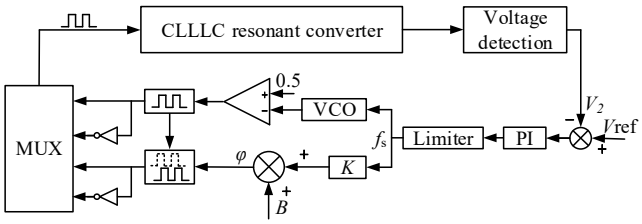

Fig.5. Block diagram of PS-PFM for CLLLC resonant converter.

B. Necessary condition for ZVS

The necessary condition for achieving ZVS for switches of primary side is that the input impedance of the resonant tank should be inductive, which means that the input current of the resonant tank lags behind the input voltage. As shown in Fig.6, θ represents the input impedance angle of the resonant tank. When θ and φ satisfy the relationship shown in equation (7), the necessary condition for ZVS of the switches can be fulfilled.

$$\theta>\frac{\varphi}{2} \tag{7}$$

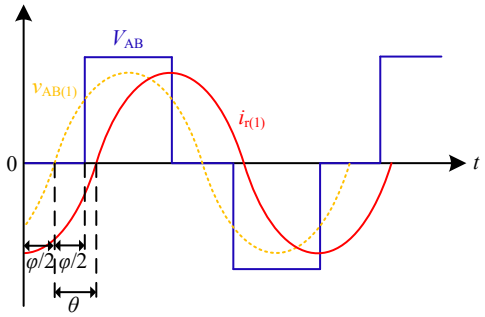

Fig.6. Key waveform diagram of PS-PFM for CLLLC resonant converter.

According to the fundamental equivalent model shown in Fig.3, the input impedance Zin of the converter can be calculated as equation (8).

$$\begin{aligned}Z_{in}&=jw_sL_1+\frac{1}{jw_sC_1}+jw_sL_m//(jw_sL_1+\frac{1}{jw_sC_1}+R_{eq}^{*})\\&=\frac{-A(w_n)+B(w_n)^2+j(A(w_n)B(w_n)Q+\frac{B(w_n)}{Q})}{Q^{-2}+B(w_n)^2}R_{eq}^{*}\end{aligned} \tag{8}$$

where

$$\begin{cases}A(w_n)=(2k+1)w_n^{2}-2k-2+\dfrac{1}{w_n^{2}}\\[2ex] B(w_n)=(k+1)w_n-\dfrac{1}{w_n}\end{cases} \tag{9}$$

Let the real part of Z_{in} be R_{in} and the imaginary part be X_{in}:

$$\begin{cases}R_{in}=\dfrac{-A(w_n)+B(w_n)^2}{Q^{-2}+B(w_n)^2}R_{eq}^{*}\\[2ex] X_{in}=\dfrac{A(w_n)B(w_n)Q+\dfrac{B(w_n)}{Q}}{Q^{-2}+B(w_n)^2}R_{eq}^{*}\end{cases} \tag{10}$$

Therefore, the impedance angle of the resonant tank can be obtained as shown in Equation (11), where w_n is the normalized angular frequency and it satisfies w_n=f_n.

$$\theta = \arctan\frac{X_{in}}{R_{in}} = \arctan\frac{QA(w_n)B(w_n)+\dfrac{B(w_n)}{Q}}{-A(w_n)+B(w_n)^2} \tag{11}$$

C. Reactive power analysis

According to equation (10), Z_{in} is composed of R_{in} and X_{in}, thus the fundamental equivalent model shown in Fig.3 can be simplified to the model shown in Fig.7.

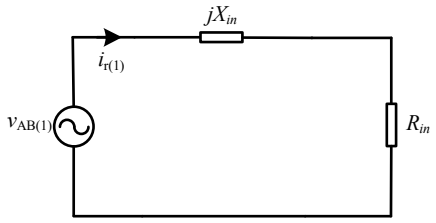

Fig.7. Simplified model diagram of fundamental harmonic equivalent model.

According to the simplified model, the active power P_o and reactive power Q_r of the converter can be calculated as follows:

$$P_o = R_{in}\left(\frac{V_{AB(1)}}{\sqrt{R_{in}^2+X_{in}^2}}\right)^2 = \frac{8R_{in}V_1^2\cos^2\dfrac{\varphi}{2}}{\pi^2\left(R_{in}^2+X_{in}^2\right)} \tag{12}$$

$$Q_r = X_{in}\left(\frac{V_{AB(1)}}{\sqrt{R_{in}^2+X_{in}^2}}\right)^2 = \frac{8X_{in}V_1^2\cos^2\dfrac{\varphi}{2}}{\pi^2\left(R_{in}^2+X_{in}^2\right)} \tag{13}$$

As seen from the above equations, when the load remains constant and the input voltage V_1 increases, both P_o and Q_r will increase accordingly, resulting in the increase of output voltage V_2. In this case, increasing the phase shift angle φ can achieve negative feedback of P_o and V_2. Therefore, the combined modulation of phase shift angle and switching frequency can reduce the range of switching frequency variation.

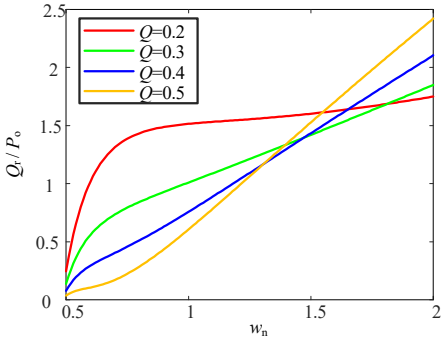

Fig.8. Diagram of Q_r/P_o as a function of w_n.

To understand the effect of the w_n on Q_r, we can derive equation (14) from equations (12) and (13). Based on this equation, we can plot the graph of the ratio of Q_r to P_o against w_n as shown in Fig.8. From the diagram, we can observe that within a certain load range, the relationship between Q_r/P_o and w_n is monotonic. Therefore, when the input voltage increases, the traditional PFM method increases the switching frequency to maintain the output voltage, resulting in higher reactive power. As mentioned earlier, PS-PFM is beneficial in reducing the range of switching frequency variation, thus improving the efficiency of the converter.

$$\frac{Q_r}{P_o} = \frac{X_{in}}{R_{in}} = \tan\theta = \frac{QA(w_n)B(w_n)+\dfrac{B(w_n)}{Q}}{-A(w_n)+B(w_n)^2} \tag{14}$$

D. Calculation of parameters K and B

As mentioned above, equation (7) is the necessary condition for achieving ZVS for the switches. By setting this equation as an equality, we obtain the critical condition for ZVS as $\theta = \frac{\varphi}{2}$. The expression for φ can be derived from equation (5) as follows:

$$\varphi = 2\arccos[M\times\sqrt{(1+\frac{1}{k}-\frac{1}{k\omega_n^2})^2+(\frac{Q}{k})^2[(2k+1)\omega_n-\frac{2k+2}{\omega_n}+\frac{1}{\omega_n^3}]^2}] \tag{15}$$

By combining equations (11), (15) and $\theta = \frac{\varphi}{2}$, equation (16) can be derived. Based on this equation, we can obtain the surface S as shown in Fig.9, which represents the critical surface of ZVS. Above the surface S, the switches can achieve ZVS, meaning that with higher switching frequency, the switches are more likely to achieve ZVS. Below the surface S, the switches lose the ZVS characteristic, meaning that with larger phase shift angle, the switches will lose the ZVS characteristic. Therefore, it is necessary to design parameters K and B according to the S plane.

$$\arctan\frac{QA(w_n)B(w_n)+\dfrac{B(w_n)}{Q}}{-A(w_n)+B(w_n)^2} = \arccos[M\times\sqrt{(1+\frac{1}{k}-\frac{1}{k\omega_n^2})^2+(\frac{Q}{k})^2[(2k+1)\omega_n-\frac{2k+2}{\omega_n}+\frac{1}{\omega_n^3}]^2}] \tag{16}$$

From Fig.8, it can be seen that when w_n is small, the increasing of Q leads to the decreasing of θ, thus the necessary condition for ZVS as shown in equation (7) becomes more difficult to achieve. In order to ensure the realization of ZVS during low-frequency and overload, point A is chosen as the calculation point for low-frequency parameters in Fig.9. As mentioned earlier, when w_n increases, θ also increases and it is more likely to achieve ZVS operation. However, excessively high switching frequency can lead to increased loss. Therefore, in order to reduce the range of switching frequency while ensuring the realization of ZVS, point B is chosen as the parameter calculation point at high frequency.

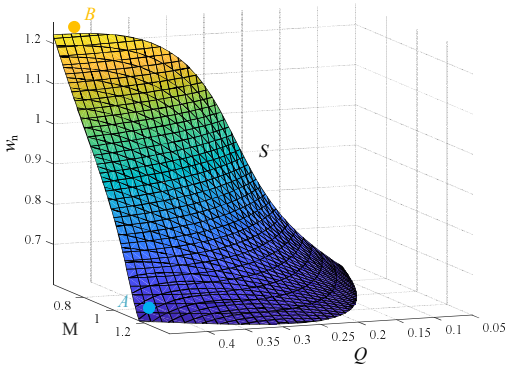

Fig.9. Diagram of ZVS critical surface.

According to equation (6), parameters K and B can be obtained from the following equation, where φ_A and φ_B can be calculated using equation (15).

$$\begin{cases} K = \dfrac{\varphi_A - \varphi_B}{f_A - f_B} \\ B = \varphi_A - K f_A \end{cases} \tag{17}$$

IV. Experimental Results

In order to verify the feasibility of the proposed PS-PFM, a simulation model was built in Matlab/Simulink software. Table I shows the parameters of the CLLLC resonant converter, and Fig.10 shows the simulation comparison between PFM and PS-PFM when V_1 is 380V. From Fig.10, it can be observed that under PFM control, the switching frequency reaches 163kHz and the secondary side body diode does not achieve ZCS, while PS-PFM has a switching frequency of 128kHz and achieves ZCS for the secondary side body diode. Therefore, PS-PFM reduces the range of switching frequency variation and achieves soft switching for the switches.

TABLE I. PARAMETERS OF THE CLLLC RESONANT CONVERTER

Parameter	Value
Primary Resonant Inductance, L_1	31.69μH
Secondary Resonant Inductance, L_2	1.56μH
Primary Resonant Capacitance, C_1	66.05nH
Secondary Resonant Capacitance, C_2	1.33μH
Magnetic Inductance, L_m	104.58μH
Transformer Turns Ratio, n:1	4.5:1
Resonance Frequency, f_r	110kHz
Parameter K	2.28e-5
Parameter B	-1.586

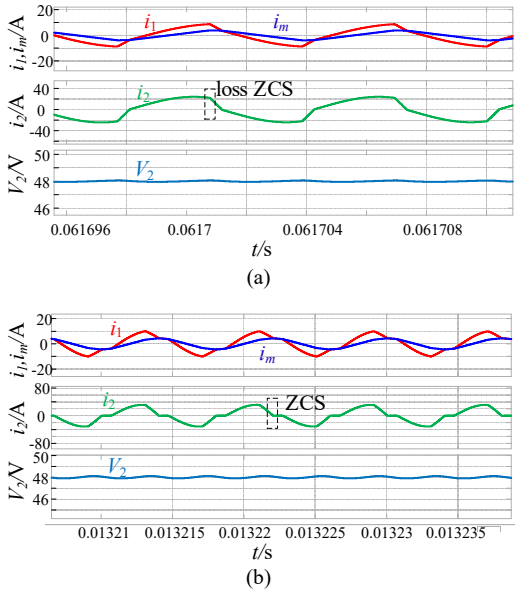

Fig.10. Simulation waveforms at V_1=380V. (a) PFM.(b) PS-PFM.

A prototype was designed to verify the effectiveness of the proposed control method. The prototype has an input voltage range of 180V to 380V, an output voltage of 48V, and a rated power of 800W. Fig.11 shows an image of the prototype, which chooses the TMS320F28377 as the digital controller and the SCTWA35N65G2V as the switch.

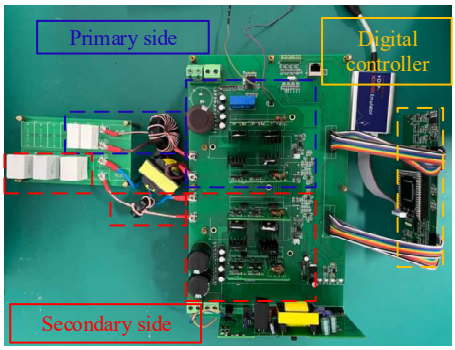

Fig.11. Experimental prototype.

The experimental waveforms for input voltage of 180V, 220V, and 380V are shown in Fig.12. From the experimental waveforms, it can be observed that the primary side resonant current lags behind the resonant tank input voltage, which means the switches of primary side achieve ZVS operation. Compared to the segmented modulation of PSM and PFM, PS-PFM does not require setting switching points and hysteresis control for two different modulation modes, simplifying the control method and therefore improving system stability.

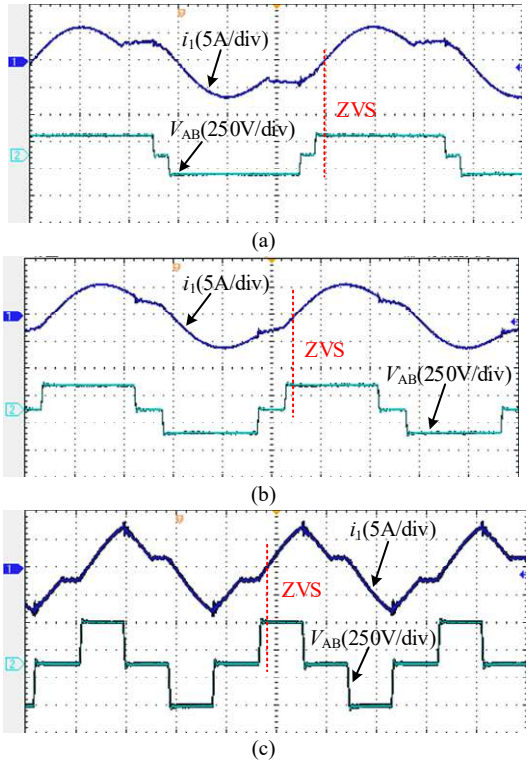

Fig.12.Experimental waveforms of PS-PFM with different input voltage.(a)V_1=180V.(b) V_1=220V. (c) V_1=380V.

V. Conclusion

This paper analyzes the necessary condition for achieving ZVS operation of the CLLLC resonant converter and designs the PS-PFM control method based on this condition. The effectiveness of this control method is demonstrated through analysis and experimentation. Compared to PFM, PSM, and the segmented modulation of PFM and PSM, this method not only significantly expands the input voltage range and reduces the variation range of the switching frequency under the premise of achieving soft switching operation, but also does not require changing modulation method according to the magnitude of voltage gain. Therefore, the efficiency of

the converter under PS-PFM control is high and more suitable for practical engineering applications.

REFERENCES

[1] T. Jiang, J. Zhang, X. Wu, K. Sheng and Y. Wang, "A Bidirectional Three-Level LLC Resonant Converter With PWAM Control," IEEE Transactions on Power Electronics, vol. 31, no. 3, pp. 2213-2225, Mar. 2016.

[2] Tao W , Wang Y , Zhang F , et al, "Pulse Frequency Modulation and Phase Shift Combined Control Method for Bidirectional LLC Resonant Converter," Transactions of China Electrotechnical Society, vol. 24, no. 33, pp. 5856-5863, Dec. 2018.

[3] Pan Haiyan, He Chao, Jiang Youming, Chen Guozhu, "Efficient variant mode control of LLC resonant converter," Electric power automation equipment, vol. 1, no. 35, pp. 71-78, Jan. 2015.

[4] Miao Zheyu,Tong Hao, Yao Wenxi, Lyu Zhengyu, "A flexible variable-mode control method for wide-range full-bridge LLC converter," Proceedings of the CSEE, vol. 2, no. 42, pp. 747-761, Jan. 2022.

[5] Miao Zheyu,Tong Hao, Yao Wenxi, Lyu Zhengyu, "Variable-mode Control Method for Wide-range Diode Clamped Bridge Paralleled LLC Converter," Jounal of Power Supply, vol. 4, no. 20, pp. 1–10, Jul. 2022.

[6] S. M. S. I. Shakib and S. Mekhilef, "A Frequency Adaptive Phase Shift Modulation Control Based LLC Series Resonant Converter for Wide Input Voltage Applications," IEEE Transactions on Power Electronics, vol. 32, no. 11, pp. 8360-8370, Nov. 2017.

[7] W. Han and L. Corradini, "Wide-Range ZVS Control Technique for Bidirectional Dual-Bridge Series-Resonant DC–DC Converters," IEEE Transactions on Power Electronics, vol. 34, no. 10, pp. 10256-10269, Oct. 2019.

[8] H. -P. Park and J. -H. Jung, "PWM and PFM Hybrid Control Method for LLC Resonant Converters in High Switching Frequency Operation," IEEE Transactions on Industrial Electronics, vol. 64, no. 1, pp. 253-263, Jan. 2017.